Production of Scalar Higgs Bosons Associated with Z^0 Boson at the CERN LHC in the MSSM

Li Lin Yang,[1] Chong Sheng Li,[1,*] Jian Jun Liu,[1] and Li Gang Jin[2]

[1]*Department of Physics, Peking University, Beijing 100871, China*

[2]*Institute of Theoretical Physics, Academia Sinica, P. O. Box 2735, Beijing 100080, China*

(Dated: February 7, 2008)

Abstract

We investigate the associated production of a scalar Higgs boson (h^0 or H^0) with Z^0 boson in the minimal supersymmetric extension of the standard model (MSSM) at the CERN Large Hadron Collider (LHC), including the contributions from $b\bar{b}$ annihilation at the tree level and gluon fusion via quark and squark loops. We quantitatively analyze the total cross sections in the mSUGRA scenario. For the production of h^0 associated with Z^0, we find that in most of the parameter regions, the contributions from initial $b\bar{b}$ and gg are at a level of one percent of the total cross section and therefore almost insignificant. For the production of H^0 associated with Z^0, the contributions from $b\bar{b}$ channel can be much larger than those from light quark initial states. Especially for large $\tan\beta$, the increment can reach about one order of magnitude. Thus, when considering the associated production of H^0 and Z^0 at the LHC, the contributions from $b\bar{b}$ annihilation should be taken into account seriously.

PACS numbers: 14.80.Cp, 12.60.Jv, 13.85.Lg

*Electronic address: csli@pku.edu.cn

I. INTRODUCTION

The search for Higgs bosons is one of the main goals of the CERN Large Hadron Collider (LHC), with $\sqrt{s} = 14$TeV and a luminosity of 100 fb^{-1} per year [1]. In the standard model (SM), the Higgs boson mass is basically a free parameter with an upper bound of $m_H \leq 600 - 800$GeV [2]. However, present data from precision measurements of electroweak quantities indicate the existence of a light Higgs boson($m_H < 204$ GeV at 95% C.L.) and direct searches rule out the case $m_H < 114$GeV [3]. In addition, in various extensions of the SM, for example, in the two-Higgs-doublet models (THDM) [4], particularly in the minimal supersymmetric standard model (MSSM) [5], there are five physical Higgs particles: two neutral CP-even bosons h^0 and H^0, one neutral CP-odd boson A^0, and two charged bosons $H^{\pm}$. The Higgs boson h^0 should be lightest, with a mass $m_{h^0} \leq 135$GeV when including the radiative corrections [6]. It has been shown [7] that the h^0 boson cannot escape detection at the LHC and that in large areas of the parameter space, more than one Higgs particle can be found.

At the LHC, the neutral Higgs bosons can be produced through following mechanisms: gluon fusion $gg \to \phi$ [8, 9, 10, 11], weak boson fusion $qq \to qqV^*V^* \to qqh^0/qqH^0$ [12], associated production with weak bosons [13], associated production with a heavy quark-antiquark pair $gg, q\bar{q} \to t\bar{t}\phi/b\bar{b}\phi$ [14] and pair production [15]. In this paper we focus our attentions on the production of h^0/H^0 in association with Z^0 boson in the MSSM. This is one of the main discovery channels of neutral Higgs bosons at the Tevatron, with the Higgs decays to $b\bar{b}$ and Z^0 decays leptonicly. The main backgrounds to this signal are $Zb\bar{b}$ production, ZZ production and top quark production [16]. At the LHC, it can be used to detect the "invisible" Higgs which decays into the LSPs. The detailed analysis of signals and backgrounds can be found in Ref. [17], where they found the ratio of signal to background can as large as 12. In the SM, the Drell-Yan production process (light $q\bar{q}$ annihilation) of Higgs associated with Z^0 boson [13], as well as the gluon fusion process [18], has been studied previously. In the MSSM, the Drell-Yan contributions are related to the ones in the SM by an overall coefficient, but the contributions of gluon fusion are generally different in the two models due to the different couplings and additional contributions from new channels. Meanwhile, there are potentially important contributions to the production of neutral Higgs bosons from $b\bar{b}$ annihilation at the tree-level. In the MSSM, the Yukawa couplings b–b–ϕ

can enhance Higgs boson production cross section via $b\bar{b}$ annihilation significantly for large $\tan\beta$. Therefore, besides the production channel via Drell-Yan process, in order to obtain the complete leading order (LO) total cross sections for the associated production of scalar Higgs bosons with Z^0 boson, the partonic subprocesses $b\bar{b} \to Zh^0/ZH^0$ should also be taken into account. Moreover, the loop induced subprocess $gg \to Zh^0/ZH^0$ become important due to the potential enhancement, and should be considered, too. We will investigate all these contributions in our work.

Our paper is organized as follows. In section II, we list analytical results for the tree level cross sections of $pp \to b\bar{b} \to Zh^0/ZH^0$ and loop induced cross sections of $pp \to gg \to Zh^0/ZH^0$ in the MSSM. In section III, we present quantitative predictions for the inclusive cross section of $pp \to Zh^0/ZH^0 + X$ at the LHC adopting the MSSM parameters constrained within the minimal supergravity (mSUGRA) scenario and discuss the implications of our results. The relevant MSSM couplings and form factors are given in the Appendix A and B, respectively.

II. CALCULATION

The relevant Feynman diagrams are created by FeynArts [19] version 3.2 automatically and are shown in Fig. 1–3. We carry out the calculation in the 't Hooft–Feynman gauge and use dimensional reduction for regularization of the ultraviolet divergences in the loop diagrams. In the following expressions, $G_{L,R}^{\bar{f}fZ}$ and G^{ijk} are the couplings, which are given explicitly in Appendix A; H stands for the scalar Higgs bosons, h^0 or H^0; S and f are propagating scalar and fermion particles, respectively.

For the partonic subprocesses

$$\begin{aligned} b(k_1) + \bar{b}(k_2) &\to Z(k_3, \varepsilon_3) + H(k_4), \\ g(k_1, \varepsilon_1) + g(k_2, \varepsilon_2) &\to Z(k_3, \varepsilon_3) + H(k_4), \end{aligned}$$

we define the Mandelstam variables as

$$\hat{s} = (k_1 + k_2)^2, \quad \hat{t} = (k_1 - k_3)^2, \quad \hat{u} = (k_1 - k_4)^2. \tag{1}$$

The tree-level amplitude $\mathcal{M}^{b\bar{b}}$ for the subprocess $b\bar{b} \to ZH$ consists of the three diagrams $(a)-(c)$ in Fig. 1. The previous results [13] for vector boson bremsstrahlung include only the

first diagram, where the $b\bar{b}$ pair replaced by light quark-antiquark pairs. We also recompute the contributions of light quarks to the tree-level cross sections and compare them with ones of $b\bar{b} \to ZH$.

Using the notations defined above, the amplitude $\mathcal{M}^{b\bar{b}}$ can be expressed as

$$\mathcal{M}^{b\bar{b}} = \mathcal{M}_a^{b\bar{b}} + \mathcal{M}_b^{b\bar{b}} + \mathcal{M}_c^{b\bar{b}} \tag{2}$$

with

$$\mathcal{M}_a^{b\bar{b}} = \bar{v}(k_2) \not{\varepsilon}_3 (G_L^{\bar{b}bZ} P_L + G_R^{\bar{b}bZ} P_R) u(k_1) \frac{-iG^{HZZ}}{\hat{s} - m_Z^2}, \tag{3}$$

$$\mathcal{M}_b^{b\bar{b}} = \sum_{S=A^0,G^0} \bar{v}(k_2) G^{b\bar{b}S} \gamma^5 u(k_1) \frac{iG^{HSZ}}{\hat{s} - m_S^2 + im_S\Gamma_S} (k_3 + 2k_4) \cdot \varepsilon_3, \tag{4}$$

$$\begin{aligned} \mathcal{M}_c^{b\bar{b}} &= \bar{v}(k_2) G^{b\bar{b}H} \frac{i(\not{k}_1 - \not{k}_3 + m_b)}{\hat{t} - m_b^2} \not{\varepsilon}_3 (G_L^{\bar{b}bZ} P_L + G_R^{\bar{b}bZ} P_R) u(k_1) \\ &+ \bar{v}(k_2) \not{\varepsilon}_3 (G_L^{\bar{b}bZ} P_L + G_R^{\bar{b}bZ} P_R) \frac{i(\not{k}_1 - \not{k}_4 + m_b)}{\hat{u} - m_b^2} G^{b\bar{b}H} u(k_1). \end{aligned} \tag{5}$$

Here $P_{L,R} \equiv (1 \mp \gamma^5)/2$, $m_{G^0} = m_Z$, $\Gamma_{G^0} = 0$, and Γ_{A^0} is the decay width of A^0.

The gluon fusion subprocess is forbidden at tree-level. At one-loop level, in general, the cross section will receive contributions from both quark loops and squark loops, as shown in Fig. 2, 3. Note that each diagram actually represents a couple of diagrams with opposite directions of charge flow. However, we find that the contributions from each pair of squark loop diagrams to this process cancel each other due to the opposite signs of momenta. So the gluon fusion cross section arises only from the quark loop diagrams, i.e.,

$$\mathcal{M}^{gg} = \mathcal{M}_a^{gg} + \mathcal{M}_b^{gg} + \cdots + \mathcal{M}_e^{gg}, \tag{6}$$

where the subscripts $a - e$ refer to the corresponding diagrams in Fig. 2.

In general, the amplitudes $\mathcal{M}^{gg}$ can be written as a linear combination of the invariants formed by three independent external momenta k_1, k_2, k_3, polarization vectors of three external gauge bosons $\varepsilon_1, \varepsilon_2, \varepsilon_3$, metric tensor $g^{\mu\nu}$ and Levi-Civita tensor $\epsilon^{\mu\nu\rho\sigma}$, in which the terms without Levi-Civita tensor vanish. Thus, with taking into account the relations $\varepsilon_1 \cdot k_1 = \varepsilon_2 \cdot k_2 = \varepsilon_3 \cdot k_3 = 0$, 24 terms remain in the amplitudes. It is easy to prove the following identity

$$\begin{aligned} g^{\mu\nu}\epsilon^{\rho\sigma\alpha\beta} &- g^{\mu\rho}\epsilon^{\nu\sigma\alpha\beta} - g^{\mu\alpha}\epsilon^{\nu\rho\sigma\beta} + g^{\mu\beta}\epsilon^{\nu\rho\sigma\alpha} \\ &+ g^{\nu\sigma}\epsilon^{\mu\rho\alpha\beta} - g^{\rho\sigma}\epsilon^{\mu\nu\alpha\beta} + g^{\sigma\alpha}\epsilon^{\mu\nu\rho\beta} - g^{\sigma\beta}\epsilon^{\mu\nu\rho\alpha} = 0. \end{aligned} \tag{7}$$

Using it, one can immediately see that not all of the 24 terms are linear independent. Actually, there are only 14 independent ones, and finally the amplitudes can be written as

$$\begin{aligned}\mathcal{M}^{gg} &= A_1\epsilon^{\varepsilon_1\varepsilon_2\varepsilon_3 k_1} + A_2\epsilon^{\varepsilon_1\varepsilon_2\varepsilon_3 k_2} + A_3\epsilon^{\varepsilon_1\varepsilon_2\varepsilon_3 k_3} + A_4\epsilon^{\varepsilon_1\varepsilon_2 k_1 k_2}\varepsilon_3\cdot k_1 + A_5\epsilon^{\varepsilon_1\varepsilon_2 k_1 k_2}\varepsilon_3\cdot k_2 \\ &+A_6\epsilon^{\varepsilon_1\varepsilon_3 k_1 k_3}\varepsilon_2\cdot k_1 + A_7\epsilon^{\varepsilon_1\varepsilon_3 k_1 k_3}\varepsilon_2\cdot k_3 + A_8\epsilon^{\varepsilon_2\varepsilon_3 k_2 k_3}\varepsilon_1\cdot k_2 + A_9\epsilon^{\varepsilon_2\varepsilon_3 k_2 k_3}\varepsilon_1\cdot k_3 \\ &+A_{10}\epsilon^{\varepsilon_1 k_1 k_2 k_3}\varepsilon_2\cdot\varepsilon_3 + A_{11}\epsilon^{\varepsilon_2 k_1 k_2 k_3}\varepsilon_1\cdot\varepsilon_3 + A_{12}\epsilon^{\varepsilon_3 k_1 k_2 k_3}\varepsilon_1\cdot\varepsilon_2 \\ &+A_{13}\epsilon^{\varepsilon_1\varepsilon_2 k_2 k_3}\varepsilon_3\cdot k_1 + A_{14}\epsilon^{\varepsilon_1\varepsilon_2 k_1 k_3}\varepsilon_3\cdot k_2.\end{aligned} \tag{8}$$

The explicit expressions of the form factors $A_i (i = 1, ..., 14)$ are shown in Appendix B.

The differential cross sections of the subprocesses are given by

$$\frac{d\hat{\sigma}}{d\hat{t}} = \frac{1}{16\pi\hat{s}(\hat{s}-4m^2)}\overline{\sum}|\mathcal{M}|^2, \tag{9}$$

where $\mathcal{M} = \mathcal{M}^{b\bar{b}}, m = m_b$ for $b\bar{b}$ channel and $\mathcal{M} = \mathcal{M}^{gg}, m = 0$ for gluon fusion.

Using the standard factorization procedure, the total cross section can be obtained as a convolution of partonic cross sections with corresponding parton distribution functions,

$$\sigma(pp\to ZH) = \sum_{\alpha,\beta}\frac{1}{1+\delta_{\alpha\beta}}\int_{\tau_0}^1 dx_1\int_{\tau_0/x_1}^1 dx_2\left[f_{\alpha/p}(x_1)f_{\beta/p}(x_2)+(\alpha\leftrightarrow\beta)\right]\hat{\sigma}(\alpha\beta\to ZH), \tag{10}$$

where $\tau_0 = (m_Z + m_H)^2/s$, $\sqrt{s}$ is the center-of-mass energy of the LHC, α and β denote the initial partons.

III. NUMERICAL RESULTS AND CONCLUSIONS

In the following we present some numerical results. In our numerical calculations, the SM input parameters were taken to be $\alpha(m_Z) = 1/128.8$, $m_W = 80.423$GeV, $m_Z = 91.188$GeV and $m_t = 174.3$GeV [3]. We use the one-loop evolution of the strong coupling constant $\alpha_s(Q)$ [20, 21] with $\alpha_s(m_Z) = 0.1172$. The leading order CTEQ6 parton distribution functions [22] are used here and the factorization scale is taken to be the invariant mass of the two final particles $\mu = m_{ZH} = \sqrt{(p_Z + p_H)^2}$. Moreover, in order to improve the perturbative calculations, we take the running mass of bottom quark $m_b(Q)$ evaluated by the one-loop formula

$$m_b(Q) = U_6(Q, m_t)U_5(m_t, m_b)m_b(m_b), \tag{11}$$

with $m_b(m_b) = 4.25$GeV. The evolution factor U_f is

$$U_f(Q_2, Q_1) = \left(\frac{\alpha_s(Q_2)}{\alpha_s(Q_1)}\right)^{d_f} \tag{12}$$

with

$$d_f = \frac{12}{33 - 2f}. \tag{13}$$

The relevant MSSM parameters, the Higgs masses and mixing angles α, are determined in the mSUGRA scenario as implemented in program package ISAJET 7.69 [23]. The GUT parameters m_0, A_0 and sgn(μ) were taken to be $m_0 = 200$ GeV, $A_0 = -100$ GeV, $\mu > 0$. $m_{1/2}$, $\tan\beta$ were varied to obtain various Higgs masses. Actually, in mSUGRA scenario, the mass of the light scalar Higgs boson h^0 can only reach about 125 GeV, which is independent of the choice of GUT parameters. It should be noted that in some parameter region, $m_{A^0} > m_Z + m_{h^0}$, and the momentum of A^0 can approach its mass shell, which will lead to a singularity arising from the A^0 propagator. This can be avoided by introduing the non-zero decay width Γ_{A^0}, which was also calculated by ISAJET.

Fig. 4(a) and 5(a) show the total cross sections for the process $pp \to Zh^0 + X$ versus the light scalar Higgs boson mass m_{h^0} for $\tan\beta = 4, 15$ and 40. Fig. 4(b) and 5(b) show the dependence of the cross sections on $\tan\beta$ for $m_{h^0} = 105$ and 115 GeV. From Fig. 4 we can see that the $b\bar{b}$ contributions are approximately one order of magnitude smaller than the ones of Drell-Yan process [13], and only increase the total cross sections by about several percents, which are smaller than the QCD corrections to the Drell-Yan process. Fig. 5 shows the contributions of gluon fusion to the cross sections. Comparing with ones of the complete $q\bar{q}$ annihilation (i.e. Drell-Yan + $b\bar{b}$), one can see that for a light h^0 (for example, $m_{h^0} = 105$ GeV), the contributions of gluon fusion are about half of the ones of the $q\bar{q}$ annihilation for low $\tan\beta(\leq 5)$, but with the increasing of $\tan\beta$ from 4 to 10, the former decrease significantly, and become one order of magnitude smaller than the latter in general. Therefore, in most of the parameter regions, the contributions of both $b\bar{b}$ and gg initial states are almost insignificant and can be neglected.

Fig. 6(a) and 7(a) show the total cross sections for the process $pp \to ZH^0 + X$ as a function of the heavy scalar Higgs boson mass m_{H^0} for the three representative values of $\tan\beta$. Fig. 6(b) and 7(b) show the dependence of the cross sections on $\tan\beta$ for $m_{H^0} = 200$ and 400 GeV. We found that the $b\bar{b}$ contributions to the total cross sections for the production of heavier neutral Higgs boson can be much larger than the contributions of Drell-Yan process

for large $\tan\beta$, as shown in Fig. 6. For example, when $\tan\beta = 40$ and $m_{H^0} = 200$ GeV, the $b\bar{b}$ cross section is about 50 fb, while one of Drell-Yan process is less than 0.5 fb. Therefore, the $b\bar{b}$ channel provides a dramatic enhancement to the total cross sections, and should definitely be considered. On the other hand, the contributions of gluon fusion are very small (< 1 fb) and can be neglected in most cases, as shown in Fig. 7.

For the comparison of the production rates of H_{SM}, h^0 and H^0, they are displayed as the functions of their masses in Fig. 8, where all the contributions (i.e. Drell-Yan + $b\bar{b}$ + gluon fusion) have been included for $\tan\beta = 4$ and 40, respectively. For the SM Higgs, as shown in Ref. [18], the gluon fusion contributions are negligible for Higgs masses allowed by experiments, so we didn't include them here. From Fig. 8, one can find that no matter what the value of $\tan\beta$ is, the production rates of H^0 are the smallest, the ones of h^0 are the largest, and the ones of H_{SM} are medium. This feature indicates that the predictions for the associated production of the Higgs bosons and Z^0 boson in the SM and the MSSM are different quantitatively and distinguishable, which is in agreement with the results shown in Ref. [21], where only Drell-Yan contributions are included.

In conclusion, we have calculated the scalar Higgs bosons (h^0, H^0) production in association with a Z^0 boson through both $b\bar{b}$ channel and gluon fusion in the mSUGRA model at the LHC. Our results show that in most of the parameter regions, the contributions to the total cross section for associated production of the light scalar Higgs boson h^0 and Z^0 boson mainly come from light quark annihilation and the contributions from initial $b\bar{b}$ and gg are small and negligible. And the total cross section for associated production of heavy scalar Higgs boson H^0 and Z^0 boson, with including the contributions of $b\bar{b}$ channel, can be increased greatly. Especially for large $\tan\beta$, such increment can reach about one order of magnitude. Thus, the contributions of $b\bar{b}$ channel should definitely be taken into account, and the ratio of signal to background obtained in Ref. [17], which is based on the previous calculations, can be enhanced at large $\tan\beta$. The contributions from gluon fusion are still small and unimportant.

Acknowledgments

This work was supported in part by the National Natural Science Foundation of China and Specialized Research Fund for the Doctoral Program of Higher Education .

APPENDIX A: COUPLINGS

Here we list the relevant couplings in the amplitudes. i, j stand for generation indices and r, s stand for color indices.

$$
\begin{aligned}
&G_L^{\bar{u}^i u^j Z} = (-3+4s_W^2)\frac{ie\delta^{ij}}{6c_W s_W}, && G_R^{\bar{u}^i u^j Z} = \frac{2ies_W\delta^{ij}}{3c_W},\\
&G_L^{\bar{d}^i d^j Z} = -(-3+2s_W^2)\frac{ie\delta^{ij}}{6c_W s_W}, && G_R^{\bar{d}^i d^j Z} = -\frac{ies_W\delta^{ij}}{3c_W},\\
&G^{h^0 ZZ} = \frac{ieM_W s_{\beta-\alpha}}{c_W^2 s_W}, && G^{H^0 ZZ} = \frac{ieM_W c_{\beta-\alpha}}{c_W^2 s_W},\\
&G^{u^i\bar{u}^j h^0} = -\frac{ic_\alpha e\delta^{ij}m_{u^i}}{2M_W s_\beta s_W}, && G^{d^i\bar{d}^j h^0} = \frac{ies_\alpha\delta^{ij}m_{d^i}}{2c_\beta M_W s_W},\\
&G^{u^i\bar{u}^j H^0} = -\frac{ies_\alpha\delta^{ij}m_{u^i}}{2M_W s_\beta s_W}, && G^{d^i\bar{d}^j H^0} = -\frac{ic_\alpha e\delta^{ij}m_{d^i}}{2c_\beta M_W s_W},\\
&G^{u^i\bar{u}^j A^0} = -\frac{e\delta^{ij}m_{u^i}}{2M_W s_W t_\beta}, && G^{d^i\bar{d}^j A^0} = -\frac{et_\beta\delta^{ij}m_{d^i}}{2M_W s_W},\\
&G^{u^i\bar{u}^j G^0} = -\frac{e\delta^{ij}m_{u^i}}{2M_W s_W}, && G^{d^i\bar{d}^j G^0} = \frac{e\delta^{ij}m_{d^i}}{2M_W s_W},\\
&G^{h^0 A^0 Z} = \frac{c_{\beta-\alpha}e}{2c_W s_W}, && G^{h^0 G^0 Z} = \frac{es_{\beta-\alpha}}{2c_W s_W},\\
&G^{H^0 A^0 Z} = -\frac{es_{\beta-\alpha}}{2c_W s_W}, && G^{H^0 G^0 Z} = \frac{c_{\beta-\alpha}e}{2c_W s_W},\\
&G^{\bar{u}_r^i u_s^j g^a} = -ig_s\delta^{ij}T^a_{rs}, && G^{\bar{d}_r^i d_s^j g^a} = -ig_s\delta^{ij}T^a_{rs}.
\end{aligned}
$$

with

$$
\begin{aligned}
&s_W = \sin\theta_W,\ c_W = \cos\theta_W,\ s_\alpha = \sin\alpha,\ c_\alpha = \cos\alpha,\ s_\beta = \sin\beta,\\
&c_\beta = \cos\beta,\ t_\beta = \tan\beta,\ s_{\beta-\alpha} = \sin(\beta-\alpha),\ c_{\beta-\alpha} = \cos(\beta-\alpha).
\end{aligned}
$$

APPENDIX B: FORM FACTORS

This appendix lists all the coefficient As in the amplitude of subprocess $gg \to ZH$, in terms of 3- and 4-points one-loop integrals[24]. The diagrams $(a)-(e)$ refer to those in Fig. 2. For convenience, we define abbreviations of one-loop integrals for each diagram as following,

$$
\begin{aligned}
C^{(a)} &= C^{(b)} = C(0,\hat{s},0,m_f^2,m_f^2,m_f^2)\\
C^{(c)} &= C(m_H^2,m_Z^2,\hat{s},m_f^2,m_f^2,m_f^2)\\
D^{(c)} &= D(0,m_H^2,m_Z^2,0,\hat{t},\hat{s},m_f^2,m_f^2,m_f^2,m_f^2)\\
C^{(d)} &= C(m_Z^2,m_H^2,\hat{s},m_f^2,m_f^2,m_f^2)
\end{aligned}
$$

$$
\begin{aligned}
D^{(d)} &= D(0, m_Z^2, m_H^2, 0, \hat{u}, \hat{s}, m_f^2, m_f^2, m_f^2, m_f^2) \\
C^{(e)} &= C(0, m_H^2, \hat{t}, m_f^2, m_f^2, m_f^2) \\
D^{(e)} &= D(m_Z^2, 0, m_H^2, 0, \hat{u}, \hat{t}, m_f^2, m_f^2, m_f^2, m_f^2)
\end{aligned}
$$

Note that in the following expressions there is an implicit sum over f for $f = t, b$.

For diagram (a) and (b), there are only two coefficients which are not zero, respectively.

$$
\begin{aligned}
A_4^{(a)} &= A_5^{(a)} = -\frac{1}{2\pi^2} G^{HZZ} (G_L^{\bar{f}fZ} - G_R^{\bar{f}fZ}) G^{\bar{f}fg_1} G^{\bar{f}fg_2} \frac{1}{\hat{s} - m_Z^2} C_{12}^{(a)} \\
A_4^{(b)} &= A_5^{(b)} = \frac{1}{2\pi^2} G^{HSZ} (G_L^{f\bar{f}S} - G_R^{f\bar{f}S}) G^{\bar{f}fg_1} G^{\bar{f}fg_2} \frac{m_f}{\hat{s} - m_S^2 + i m_S \Gamma_S} C_0^{(b)}
\end{aligned}
$$

For diagram (c), the coefficients are the following expressions time an overall factor $\frac{1}{8\pi^2} G^{f\bar{f}H} (G_L^{\bar{f}fZ} - G_R^{\bar{f}fZ}) G^{\bar{f}fg_1} G^{\bar{f}fg_2} m_f$

$$
\begin{aligned}
A_1 &= 4\left[C_0^{(c)} + C_1^{(c)} + C_2^{(c)} - 2D_{00}^{(c)} + \hat{s}(D_{12}^{(c)} + D_{13}^{(c)})\right] \\
&\qquad + (\hat{u} - m_Z^2)\left[D_0^{(c)} - 2D_2^{(c)} + 4(D_{22}^{(c)} + D_{23}^{(c)})\right] \\
A_2 &= 2C_0^{(c)} + 4(C_1^{(c)} + C_2^{(c)}) + (\hat{t} - m_Z^2) D_0^{(c)} - 2\hat{s} D_1^{(c)} \\
&\qquad + 8D_{00}^{(c)} + 4(m_Z^2 + \hat{s} - \hat{t}) D_{12}^{(c)} + 4\hat{s} D_{13}^{(c)} \\
A_3 &= -2C_0^{(c)} - 4C_1^{(c)} + \hat{s}\left[D_0^{(c)} - 2D_2^{(c)} - 4(D_{12}^{(c)} + D_{22}^{(c)} + D_{23}^{(c)})\right] \\
A_4 &= -4\left[D_0^{(c)} + D_2^{(c)} + D_3^{(c)} - 2(D_{12}^{(c)} + D_{13}^{(c)})\right] \\
A_5 &= 4\left[D_1^{(c)} + 2(D_{12}^{(c)} + D_{13}^{(c)})\right] \\
A_6 &= 4\left[D_2^{(c)} + D_3^{(c)} + 2(D_{22}^{(c)} + D_{23}^{(c)})\right] \\
A_7 &= A_9 = -4(D_2^{(c)} + 2D_{22}^{(c)}) \\
A_8 &= -4(D_1^{(c)} + 2D_{12}^{(c)}) \\
A_{10} &= 2(D_0^{(c)} - 2D_3^{(c)} - 4D_{12}^{(c)}) \\
A_{11} &= -2\left[D_0^{(c)} + 4D_2^{(c)} - 2D_3^{(c)} + 4(D_{22}^{(c)} + D_{23}^{(c)})\right] \\
A_{12} &= -2\left[D_0^{(c)} - 2D_2^{(c)} - 4(D_{12}^{(c)} + D_{22}^{(c)} + D_{23}^{(c)})\right] \\
A_{13} &= -4(D_0^{(c)} + D_2^{(c)} - D_3^{(c)} - 2D_{12}^{(c)}) \\
A_{14} &= 4\left[D_2^{(c)} - D_3^{(c)} + 2(D_{22}^{(c)} + D_{23}^{(c)})\right]
\end{aligned}
$$

The overall factor for diagram (d) is $\frac{1}{8\pi^2} G^{f\bar{f}H} (G_L^{\bar{f}fZ} - G_R^{\bar{f}fZ}) G^{\bar{f}fg_1} G^{\bar{f}fg_2} m_f$, and the coef-

ficients are

$$
\begin{aligned}
A_1 &= -2C_0^{(d)} + 4C_2^{(d)} + (m_Z^2 - \hat{u} - 4)D_0^{(d)} + 2\hat{s}D_3^{(d)} \\
&\qquad +8D_{00}^{(d)} + 4(\hat{u} - m_Z^2)D_{12}^{(d)} + 4\hat{u}D_{22}^{(d)} + 4(\hat{u} - \hat{t})D_{23}^{(d)} \\
A_2 &= 4C_2^{(d)} + (m_Z^2 - \hat{t})\left[D_0^{(d)} - 2D_2^{(d)} - 4(D_{12}^{(d)} + D_{22}^{(d)})\right] + 8D_{00}^{(d)} - 4\hat{s}(D_{13}^{(d)} + D_{23}^{(d)}) \\
A_3 &= 2C_0^{(d)} + 4C_1^{(d)} - \hat{s}\left[D_0^{(d)} - 2D_2^{(d)} - 4(D_{12}^{(d)} + D_{22}^{(d)} + D_{22}^{(d)})\right] \\
A_4 &= 4\left[D_3^{(d)} + 2(D_{13}^{(d)} + D_{23}^{(d)})\right] \\
A_5 &= -4\left[D_0^{(d)} + D_1^{(d)} + D_2^{(d)} - 2(D_{13}^{(d)} + D_{23}^{(d)})\right] \\
A_6 &= -4(D_3^{(d)} + 2D_{23}^{(d)}) \\
A_7 &= A_9 = -4(D_2^{(d)} + 2D_{22}^{(d)}) \\
A_8 &= 4\left[D_1^{(d)} + D_2^{(d)} + 2(D_{12}^{(d)} + D_{22}^{(d)})\right] \\
A_{10} &= -2\left[D_0^{(d)} - 4(D_2^{(d)} + D_{12}^{(d)} + D_{22}^{(d)})\right] \\
A_{11} &= 2(D_0^{(d)} + 4D_{23}^{(d)}) \\
A_{12} &= 2\left[D_0^{(d)} - 2D_2^{(d)} - 4(D_{12}^{(d)} + D_{22}^{(d)} + D_{23}^{(d)})\right] \\
A_{13} &= 2\left[D_0^{(d)} - D_1^{(d)} - 2D_2^{(d)} - 4(D_{12}^{(d)} + D_{22}^{(d)})\right] \\
A_{14} &= 4(D_2^{(d)} - 2D_{23}^{(d)})
\end{aligned}
$$

For diagram (e), the overall factor is $\frac{1}{8\pi^2}G^{f\bar{f}H}(G_L^{\bar{f}fZ} - G_R^{\bar{f}fZ})G^{\bar{f}fg_1}G^{\bar{f}fg_2}m_f$, and coefficients are

$$
\begin{aligned}
A_1 &= -2C_0^{(e)} + (\hat{u} - m_Z^2)D_0^{(e)} + 2(m_Z^2 + \hat{u})D_1^{(e)} + 4\hat{u}D_2^{(e)} + (m_Z^2 + \hat{s} - \hat{u})D_3^{(e)} + 8D_{00}^{(e)} \\
&\qquad +4m_Z^2 D_{11}^{(e)} + 4(m_Z^2 + \hat{u})(D_{12}^{(e)} + D_{22}^{(e)}) + 4(\hat{u} - m_Z^2)D_{13}^{(e)} + \left[4(\hat{u} - m_Z^2) - \hat{s}\right]D_{23}^{(e)} \\
A_2 &= -2C_0^{(e)} + 8D_{00}^{(e)} + 2(\hat{t} - m_Z^2)\left[D_1^{(e)} + D_2^{(e)} + 2(D_{12}^{(e)} + D_{22}^{(e)})\right] - 4\hat{s}D_{23}^{(e)} \\
A_3 &= 2\hat{s}\left[D_1^{(e)} + 3D_2^{(e)} + 2(D_{13}^{(e)} + D_{23}^{(e)})\right] + 2(2\hat{s} - m_Z^2)D_{12}^{(e)} + (\hat{t} - m_Z^2 + 5\hat{s})D_{22}^{(e)} \\
A_4 &= 4(D_3^{(e)} + 2D_{23}^{(e)}) \\
A_5 &= 4(D_2^{(e)} + 2D_{23}^{(e)}) \\
A_6 &= -4\left[D_3^{(e)} + 2(D_{13}^{(e)} + D_{23}^{(e)})\right] \\
A_7 &= -4\left[D_0^{(e)} + 3(D_1^{(e)} + D_2^{(e)}) + 2(D_{11}^{(e)} + 2D_{12}^{(e)} + D_{22}^{(e)})\right] \\
A_8 &= 4\left[D_2^{(e)} + 2(D_{12}^{(e)} + D_{22}^{(e)})\right]
\end{aligned}
$$

$$
\begin{aligned}
A_9 &= -4\left[D_1^{(e)} + D_2^{(e)} + 2(D_{11}^{(e)} + 2D_{12}^{(e)} + D_{22}^{(e)})\right] \\
A_{10} &= 8(D_2^{(e)} + D_{12}^{(e)} + D_{22}^{(e)}) \\
A_{11} &= 8(D_{13}^{(e)} + D_{23}^{(e)}) \\
A_{12} &= -2\left[D_0^{(e)} + 2D_1^{(e)} + 6D_2^{(e)} + 4(D_{12}^{(e)} + D_{22}^{(e)} + D_{13}^{(e)} + D_{23}^{(e)})\right] \\
A_{13} &= -4\left[D_1^{(e)} + 3D_2^{(e)} + 2(D_{12}^{(e)} + D_{22}^{(e)})\right] \\
A_{14} &= -2\left[D_0^{(e)} + 2(D_1^{(e)} + D_2^{(e)}) + 4(D_{13}^{(e)} + D_{23}^{(e)})\right]
\end{aligned}
$$

---

[1] F. Gianotti, M. L. Mangano and T. Virdee, CERN-TH/2002-078, hep-ph/0204087.

[2] T. Hambye and K. Riesselmann, Phys. Rev. **D55**, 7255 (1997).

[3] Particle Data Group (K. Hagiwara *et al.*), Phys. Rev. **D66**, 010001 (2002).

[4] N. G. Deshpande and E. Ma, Phys. Rev. **D18**, 2574 (1978); H. Geogi, Hadronic Journal **1**, 155 (1978); H. E. Haber, G. L. Kane and T. Sterling, Nucl. Phys. **B161**, 493 (1979); J. F. Donoghue and L. F. Li, Phys Rev. **D19**, 945 (1979); L. F. Abbott, P. Sikivie and M. B. Wise, Phys. Rev. **D21**, 1393 (1980); B. McWilliams and L. F. Li, Nucl. Phys. **B179**, 62 (1981).

[5] H. E. Haber and G. L. Kane, Phys. Rep. **117**, 75 (1985).

[6] H. E. Haber and R. Hempfling, Phys. Rev. Lett. **66**, 1815 (1991); Y. Okada, M. Yamaguchi and T. Yanagida, Prog. Theor. Phys. **85**, 1 (1991); J. Ellis, G. Ridolfi and F. Zwirner, Phys. Lett. **B257**, 83 (1991).

[7] A. Djouadi, CERN TH/2003-043, hep-ph/0303097; M. Dittmar, talk given at WHEPP 1999, Pramana 55, 151 (2000); F. Gianotti, talk given at the LHC Committee Meeting, CERN, 5/7/2000.

[8] H. Georgi *et al.*, Phys. Rev. Lett. **40**, 692 (1978).

[9] M. Spira, A. Djouadi, D. Graudenz and P. Zerwas, Phys. Lett. **B318**, 347 (1993); Nucl. Phys. **B453**, 17 (1995); S. Dawson, A. Djouadi and M. Spira, Phys. Rev. Lett. **77**, 16 (1996); A. Djouadi and M. Spira, Phys. Rev. **D62**, 014004 (2000).

[10] R. V. Harlander and W. Kilgore, Phys. Rev. Lett. **88**, 201801 (2002); J. High Energy Phys. **0210**, 017 (2002); C. Anastasiou and K. Melnikov, Nucl. Phys. **B646**, 220 (2002); Phys. Rev. D67, 037501 (2003); V. Ravindran, J. Smith and W. L. van Neerven, Nucl. Phys. **B665**, 325 (2003).

[11] S. Catani, D. de Florian, M. Grazzini and P. Nason, J. High Energy Phys. **0307**, 028 (2003); A. Kulesza, G. Sterman and W. Vogelsang, hep-ph/0309264.

[12] R. N. Cahn and S. Dawson, Phys. Lett. **B136**, 196 (1984); G. Altarelli, B. Mele and F. Pitolli, Nucl. Phys. **B287**, 205 (1987); T. Han, G. Valencia and S. Willenbrock, Phys. Rev. Lett. **69**, 3274 (1992).

[13] S. L. Glashow, D. V. Nanopoulos and A. Yildiz, Phys. Rev. **D18**, 1724 (1978); R. Kleiss, Z. Kunszt and W. J. Stirling, Phys. Lett. **B253**, 269 (1991); T. Han and S. Willenbrock, Phys. Lett. **B273**, 167 (1991).

[14] Z. Kunszt, Nucl. Phys. **B247**, 339 (1984); W. Beenakker *et al.*, Phys. Rev. Lett. **87**, 201805 (2001); Nucl. Phys. **B653**, 151 (2003); S. Dawson *et al.*, Phys. Rev. Lett. **87**, 201804 (2001); Phys. Rev. **D67**, 071503 (2003).

[15] A. A. Barrientos Bendezú and B. A. Kniehl, Phys. Rev. **D64**, 035006 (2001).

[16] M. Carena *et al.*, hep-ph/0010338.

[17] D. Choudhury and D. P. Roy, Phys. Lett. **B322**, 368 (1994); R. M. Godbole, M. Guchait, K. Mazumdar, S. Moretti, and D. P. Roy, Phys. Lett. **B571**, 184 (2003).

[18] B. A. Kniehl, Phys. Rev. **D42**, 2253 (1990).

[19] T. Hahn, Comp. Phys. Comm. **140**, 418 (2001).

[20] S. G. Gorishny *et al.*, Mod. Phys. Lett. **A5**, 2703 (1990); Phys. Rev. **D43**, 1633 (1991); A. Djouadi, M. Spira and P. M. Zerwas, Z. Phys. **C70**, 427 (1996); A. Djouadi, J. Kalinowski and M. Spira, Comput. Phys. Commun. **108**, 56 (1998).

[21] M. Spira, Fortschr. Phys. **46**, 203 (1998).

[22] J. Pumplin, D. R. Stump, J. Huston, H. L. Lai, P. Nadolsky and W. K. Tung, J. High Energy Phys. **0207**, 012 (2002).

[23] H. Baer *et al.*, Manual of ISAJET version 7.69 at `http://www.phy.bnl.gov/~isajet`; hep-ph/0001086 (1999).

[24] G. Passarino and M. Veltman, Nucl. Phys. **B160**, 151 (1979); A. Denner, Fortschr. Phys. **41**, 4 (1993).

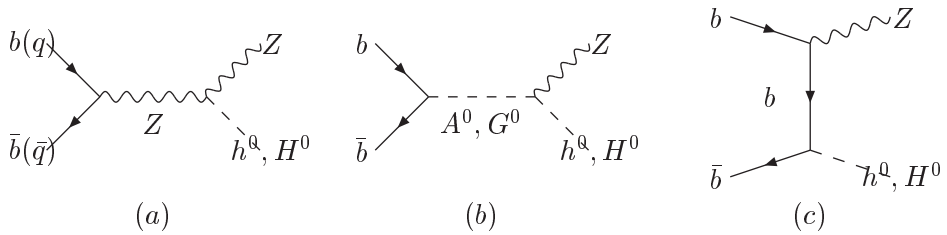

FIG. 1: Feynman diagrams for the subprocess $b\bar{b} \to ZH$

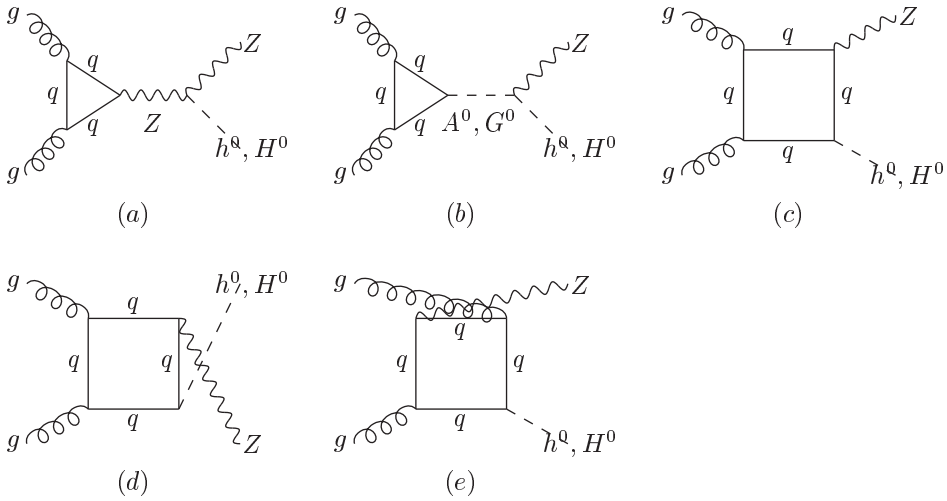

FIG. 2: Feynman diagrams for the subprocess $gg \to ZH$ (including only quark loop)

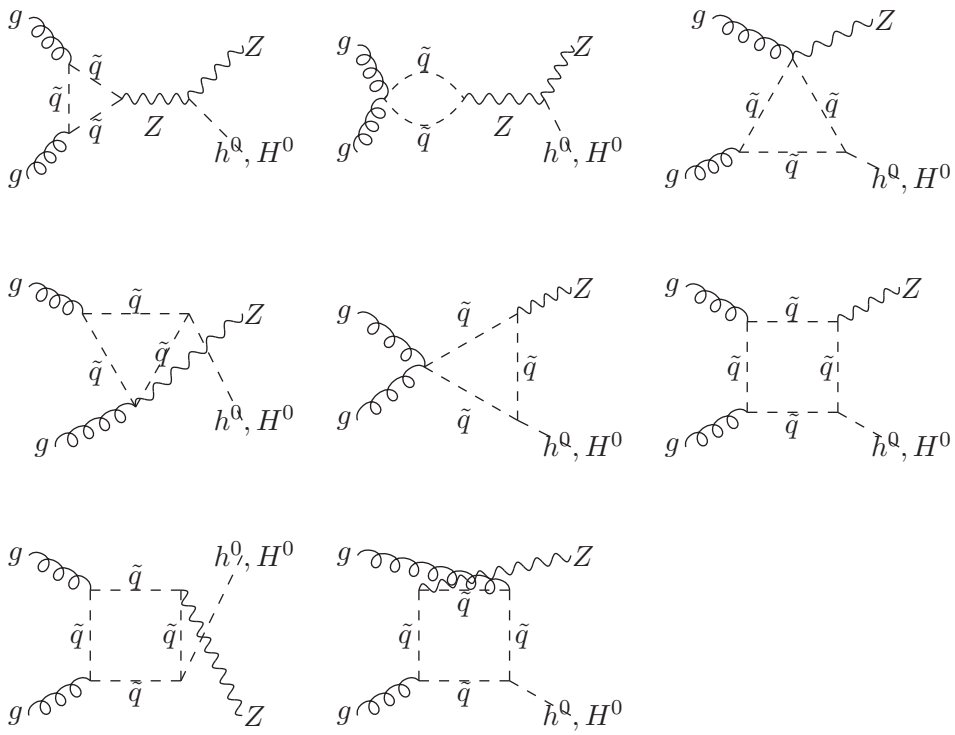

FIG. 3: Feynman diagrams for the subprocess $gg \to ZH$ (including only squark loop)

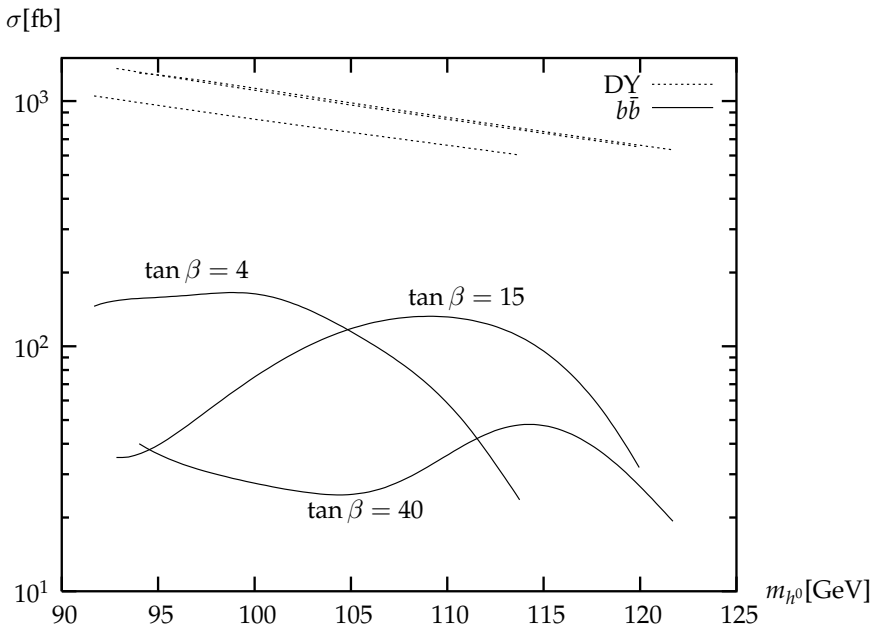

(a)

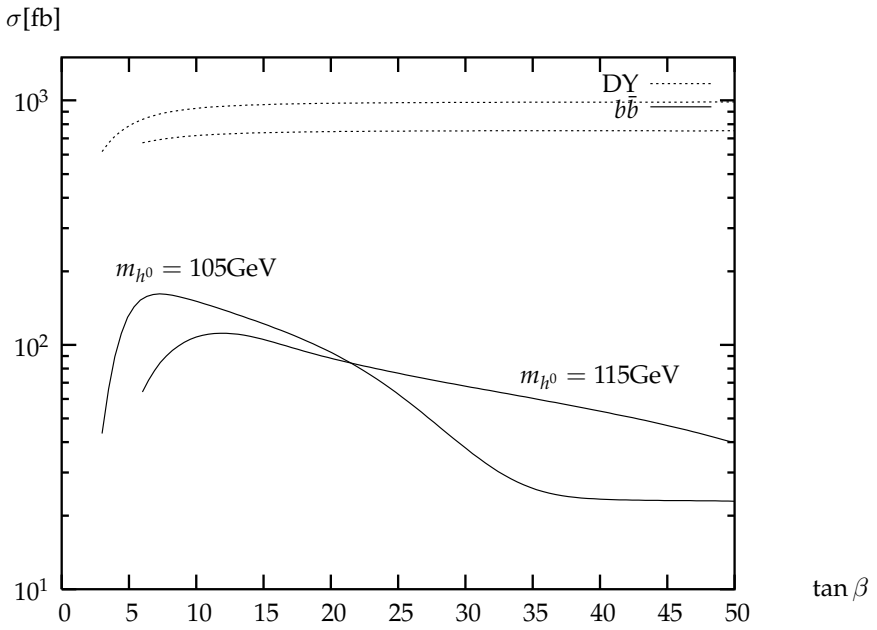

(b)

FIG. 4: Total cross sections σ (in fb) of $pp \to Zh^0$ via $b\bar{b}$ annihilation (solid lines) compared with Drell-Yan ones (dotted lines) at the LHC (a) as functions of m_{h^0} for $\tan\beta = 4$, 15 and 40; and (b) as functions of $\tan\beta$ for $m_{h^0} = 105$ and 115 GeV.

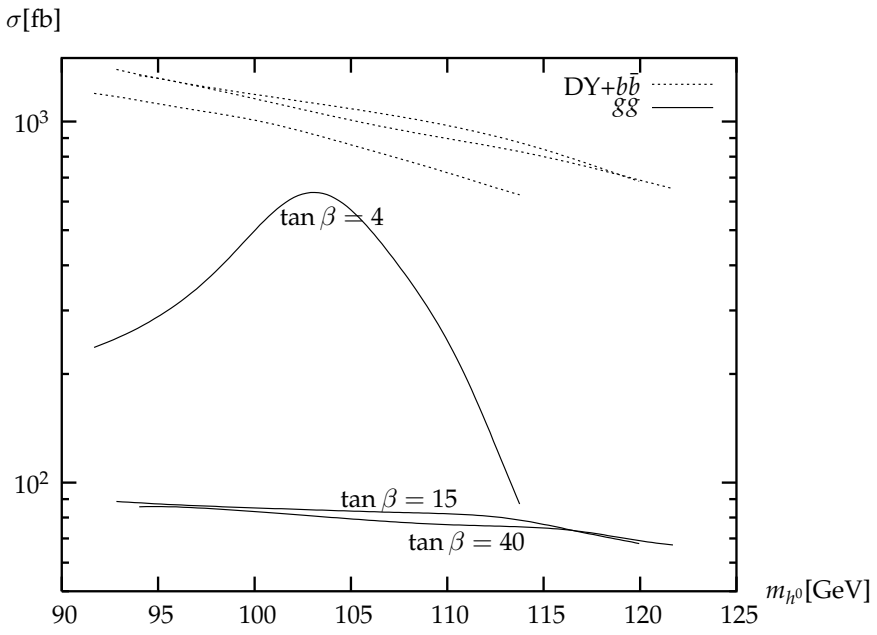

(a)

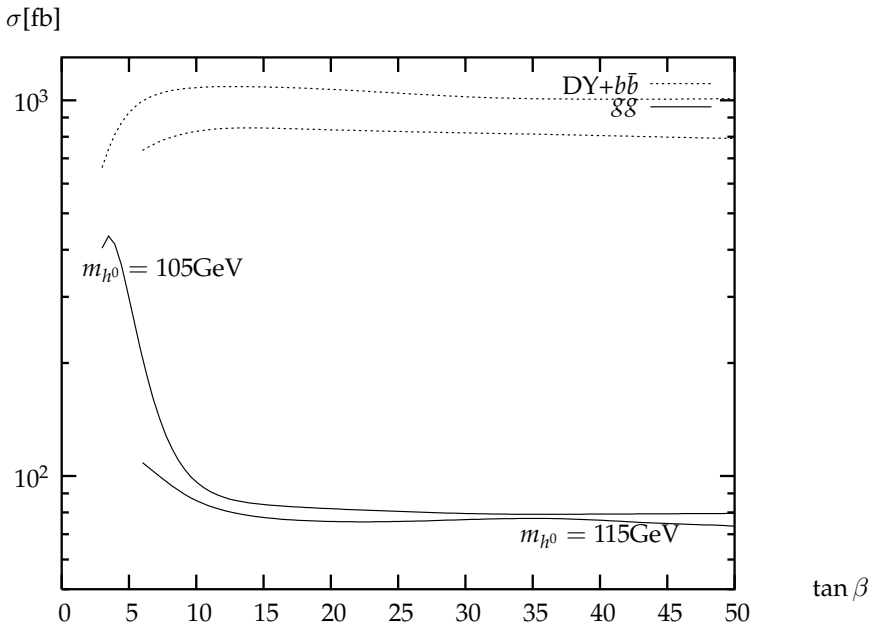

(b)

FIG. 5: Total cross section σ (in fb) of $pp \to Zh^0$ via gluon fusion (solid lines) compared with complete $q\bar{q}$ annihilation ones (dotted lines) at the LHC (a) as functions of m_{h^0} for $\tan\beta = 4$, 15 and 40; and (b) as functions of $\tan\beta$ for $m_{h^0} = 105$ and 115 GeV.

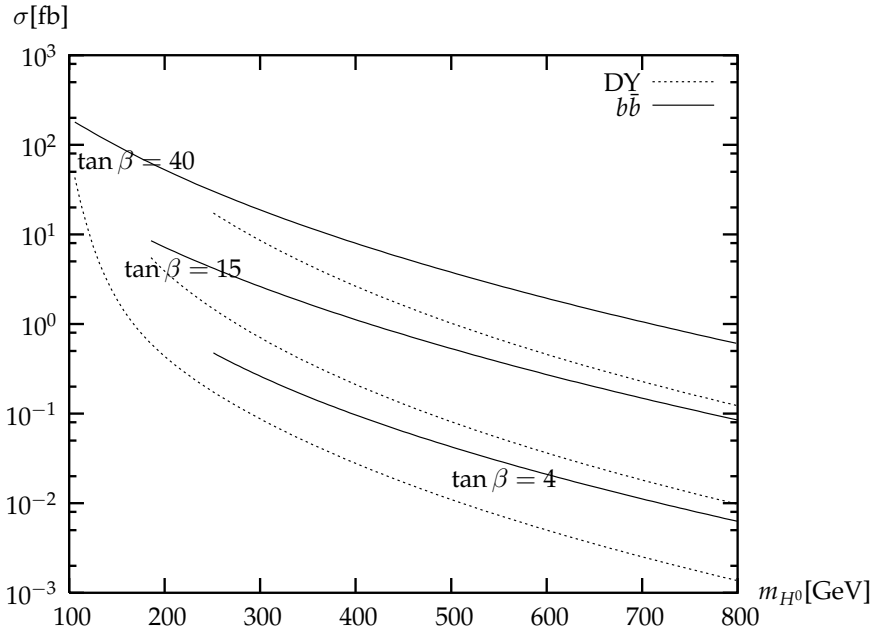

(a)

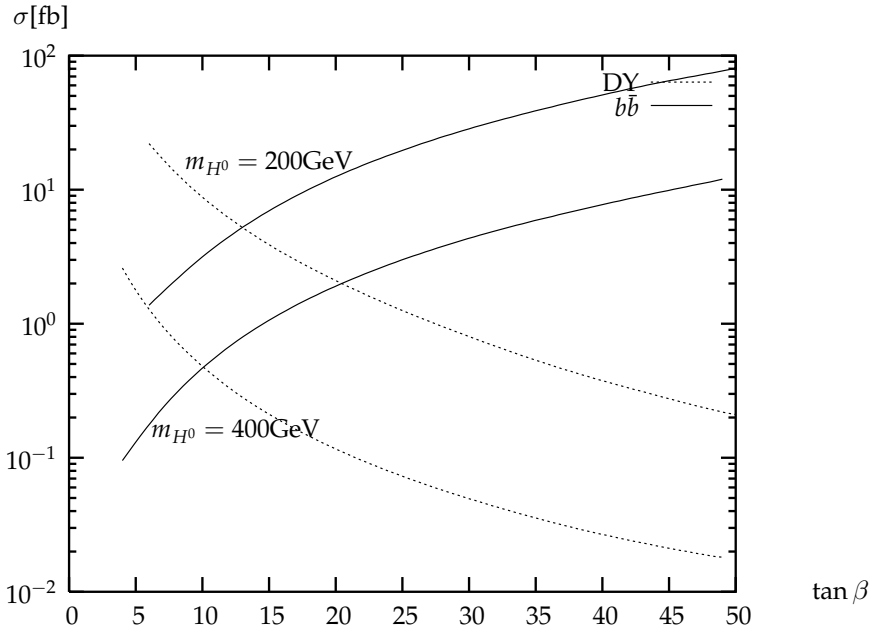

(b)

FIG. 6: Total cross sections σ (in fb) of $pp \to ZH^0$ via $b\bar{b}$ annihilation (solid lines) compared with Drell-Yan ones (dotted lines) at the LHC (a) as functions of m_{H^0} for $\tan\beta = 4$ (curves starting from m_{H^0}=250GeV, 15 (curves starting from m_{H^0}=200GeV and 40 (curves starting from m_{H^0}=100GeV); and (b) as functions of $\tan\beta$ for $m_{H^0} = 200$ and 400 GeV.

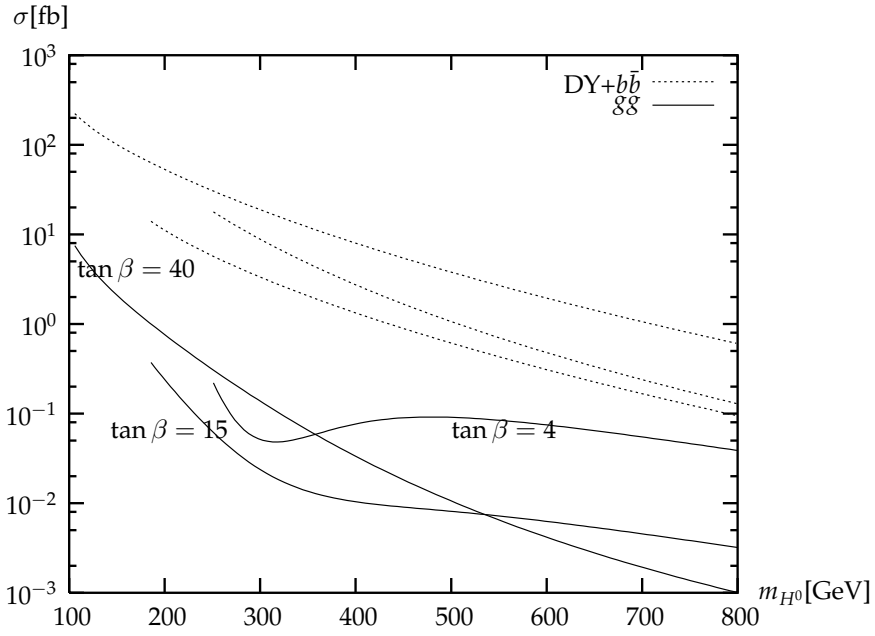

(a)

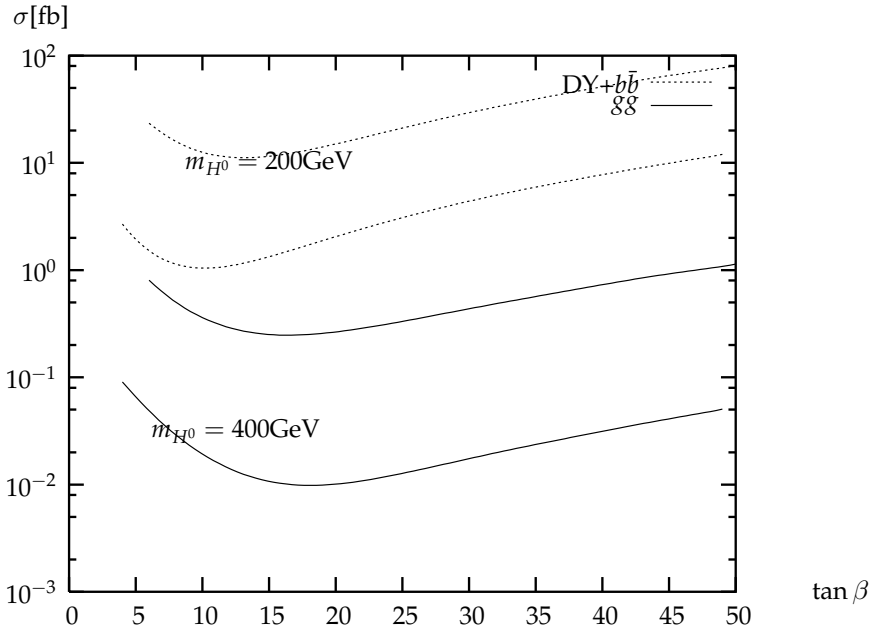

(b)

FIG. 7: Total cross section σ (in fb) of $pp \to ZH^0$ via gluon fusion (solid lines) compared with complete $q\bar{q}$ annihilation ones (dotted lines) at the LHC (a) as functions of m_{H^0} for $\tan\beta = 4$, 15 and 40(the mass ranges are the same as Fig. 6); and (b) as functions of $\tan\beta$ for $m_{H^0} = 200$ and 400 GeV.

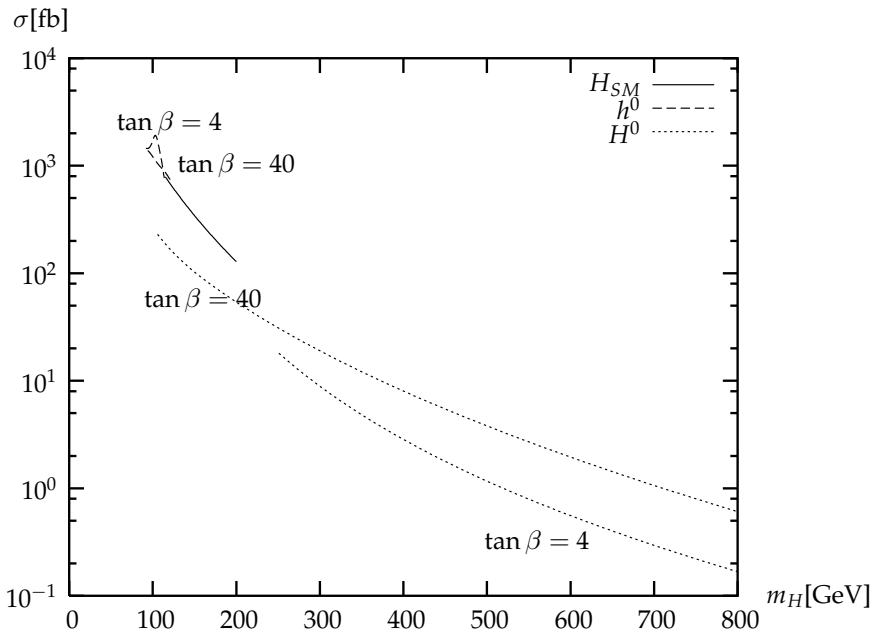

FIG. 8: A comparison of the production cross sections of the three Higgs bosons as functions of their masses.